N78-10145

Contents

2. A Charging Model for Three-Axis Stabilized Spacecraft

M. J. Massaro, T. Green, and D. Ling
General Electric Company
Space Division
Philadelphia, Pa.

Abstract

A charging model is developed for geosynchronous, three-axis stabilized spacecraft when under the influence of a geomagnetic substorm. The differential charging potentials between the thermally coated or blanketed outer surfaces and metallic structure of a spacecraft are determined when the spacecraft is immersed in a dense plasma cloud of energetic particles. The spacecraft-to-environment interaction is determined by representing the charged particle environment by equivalent current source forcing functions and by representing the spacecraft by its electrically equivalent circuit with respect to the plasma charging phenomenon. The charging model includes a sun/earth/spacecraft orbit model that simulates the sun illumination conditions of the spacecraft outer surfaces throughout the orbital flight on a diurnal as well as a seasonal basis. Transient and steady-state numerical results for a three-axis stabilized spacecraft are presented.

I. INTRODUCTION

Recent data from the geosynchronous orbiting NASA satellites ATS-5 and ATS-6[1,2,3] has indicated that the surface of these satellites can charge to hundreds of volts when in sunlight and thousands of volts (up to -10 kV) when in eclipse. Data transmitted from these satellites during these charging events has indicated the existence of transient fluxes of energetic particles. It has been suggested[4] that these clouds of energetic particles are injected into the local-midnight-to-dawn region of the geosynchronous altitude during geomagnetic substorm activity. Consequently, during a geomagnetic substorm, spacecraft at altitudes greater than three Earth radii, in the local time sector from just before midnight to past dawn, occasionally will encounter and be immersed in a dense plasma cloud of energetic particles. It has been further postulated that this charged particle environment is the major cause of spacecraft charging. That is, in the steady-state, every isolated part of a spacecraft immersed in the space environmental plasma will come into electrical equilibrium by developing surface charges of the proper sign and magnitude such that the net current — represented by the deposition and release of charged particles from the surface of the spacecraft — is zero. The equilibrium potential of the surface of the spacecraft is the potential difference between the surface and ambient plasma sheath. The most important contributors to the equilibration currents are the primary plasma electron and proton arrivals at the surface and the photoelectrons released when sunlight illuminates the surface. In addition, the contributions of secondary electrons released from the surface under primary proton or electron impact and possible electron reattraction to the surface, are also significant and must be considered in a complete analysis of the problem.

In the coincidence with the geomagnetic substorm activity in this local time quadrant, is the occurrence of anomalous events on-board satellites in geosynchronous orbit when immersed in the substorm plasma. Specifically, anomalous behavior experienced by several satellites has included[5] control circuit switching, power system failure, sensor data noise, thermal control degradation, and telemetry logic switching. There is a growing body of evidence which demonstrates the dependence of satellite anomalous behavior on geophysical parameters such as local time and geomagnetic activity.

Consequently, it has been postulated[1,4] that the anomalous behavior of synchronous spacecraft is due to electrostatic charging of the various spacecraft surfaces to large negative potentials and their subsequent discharging. The electromagnetic pulses produced by the discharges contain enough energy to interact with electronic logic circuits at distances of tens of centimeters, and cause voltage spikes large enough to change logic states. Other data from spacecraft indicate that repeated discharging also results in the degradation of thermal control surfaces.

Thus, it is the differential charging of the various thermally blanketed or coated outer surface materials with respect to each other and with respect to the spacecraft metallic structure and the subsequent discharging, when the dielectric strength of the surface materials is exceeded, that is one of the major causes of satellite anomalous behavior.

The purpose of this paper is to develop a spacecraft charging simulation model which adequately represents the spacecraft-to-environment interaction when the spacecraft is immersed in the charged particle environment that is encountered at geosynchronous orbit during a geomagnetic substorm. Further, the principal results of the simulation analysis model developed will be the differential charging potentials between the thermally blanketed or coated outer surfaces and the metallic structure of the spacecraft. To determine the spacecraft-to-environment interaction, the equivalent electrical model of the spacecraft with respect to the charging phenomenon is developed and the plasma environment is represented by equivalent current forcing functions. The equivalent current sources of the charged particle environment simulate the ambient plasma as a charging current source and the surface photoelectron and secondary electron emissions as discharging current sources. The spacecraft outer surface configuration is represented by constituent dielectric and metallic surfaces which collect charge from the environment. In addition, a S/C geometrical model and a solar/earth orbital model are also developed to determine the sun-illumination condition of the outer surfaces as a function of spacecraft orbital position. That is, the geometrical and orbital models are used to determine whether a surface is sun-illuminated, self-shadowed, or earth-shadowed. In addition, when a surface is sun-illuminated, the intensity of the illumination, which is a function of the sun/spacecraft surface aspect angle, is also determined by the models.

Charging models have appeared recently in the literature.[2, 6, 7] However, the models are based primarily on the analysis of spin-stabilized spacecraft. For the particular types of spacecraft analyzed, there was considerable seasonal and diurnal variation of the exposed metallic area illuminated by the sun. However, due to the restricted location of thermal blanket materials and the external structural form of spin-stabilized spacecraft, there were small diurnal variations in both the amount and location of the thermal blanket material areas illuminated by the sun during the midnight-to-dawn local time quadrant. Consequently, no attempt was made to determine the sun-illumination condition of exposed dielectric surfaces during the daily orbital flight. However, for three-axis stabilized spacecraft the diurnal as well as the seasonal variations of the amount and location of both the dielectric and exposed metallic areas illuminated by the sun are considerable. The model discussed in this paper determines the variations of sun-illumination condition of all of the exposed surfaces throughout the daily orbital path in addition

to considering the seasonal changes. Also, the previous models have not considered the intrinsic capacitance of the spacecraft structure with respect to the plasma sheath. In this paper, the structural capacitance has been included in the simulation model, and it will be shown that the structural capacitance has a significant influence on the transient response.

In the following sections, the development of the spacecraft charging model is discussed in general terms and includes a discussion of the plasma model, the electrical model, the geometrical model, a solar/earth orbital model, the material properties and configuration definition, and the numerical integration approach. Spacecraft charging results are given for a geosynchronous satellite during the midnight-to-dawn local time quadrant for the fall-equinox and winter-solstice seasonal periods.

2. SPACECRAFT CHARGING MODEL DEVELOPMENT

The spacecraft charging model development can best be described in terms of the flow chart shown in Figure 1. The S/C charging model consists of four separate models: a plasma model, an electrical model, a S/C geometrical model: and a solar/earth orbital model. The plasma model represents the charging and discharging mechanism of the ambient plasma with respect to the spacecraft by equivalent current sources. The current sources, which are dependent on the particle energy distribution functions, constitute the forcing functions of the charging model equations. The electrical model defines the lumped element equivalent circuit representation of the spacecraft surfaces with respect to the electrostatic charging phenomenon. The plasma model and electrical model are combined to form the nonlinear spacecraft charging equations. The spacecraft geometrical model defines the spacecraft outer surfaces in terms of approximate planar surfaces and curved surface projections and defines the vertices of all planar and curved surfaces in terms of a spacecraft reference coordinate system. The solar/earth orbital model determines the location of the spacecraft with respect to the sun and the earth. The geometrical model and the solar/earth orbital model are combined to determine the variation of the sun-illumination conditions of the outer surfaces with respect to orbital position.

To complete the modeling, the surface material properties and configuration are defined. The surface material properties that are most important in a spacecraft charging analysis are: the relative dielectric constant, the variation of the surface resistivity with respect to electrical stress level, and the variation of the bulk resistivity with respect to electrical stress level. The material configuration definition describes the location of the various thermal blanket and surface coating materials.
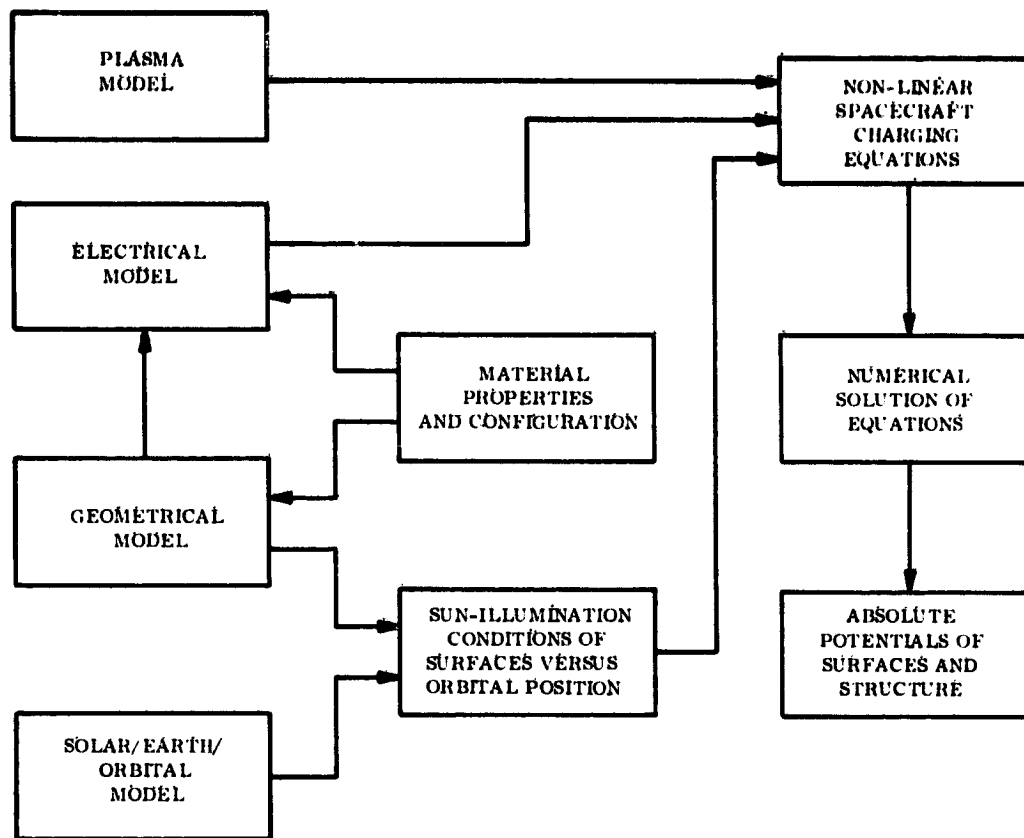
240

Figure 1. Spacecraft Charging Model Flow Chart

The elements of the flow chart will now be discussed in greater detail.

2.1 Plasma Model

As discussed previously, spacecraft at geosynchronous orbit will occasionally encounter energetic charged particle fluxes and these fluxes will cause the various outer surfaces to charge to large potentials. The charging and discharging mechanism of the ambient plasma with respect to the spacecraft can be represented or simulated by equivalent current sources that become the forcing functions of the charging model equations. The constituent particle fluxes that affect the charging of a surface are protons, electrons, photoelectrons, and secondary electrons.

Several investigators[6,8,9] have approximated the energy distribution of the particle fluxes as measured on ATS-5 by a Maxwell-Boltzmann (M-B) energy distribution and, further, have assumed the particle fluxes to have an omnidirectional energy distribution; that is, the energy distribution of the particles is identical in

241

each direction. Thus, it is possible to characterize the particle energy distributions by a thermal energy (Kτ) expressed in electron volts. This approximation is used in this paper to simplify the analysis and to provide an insight into the problem that might otherwise be obscured by a more complex approach.

The total current flowing into the outer surface of a spacecraft is

$$I = J_T \cdot A \tag{1}$$

where A is the surface area and J_T is the total positive current density into the surface and is given by

$$J_T = J_p + J_{sp} - J_e + J_{se} + J_{ph} \tag{2}$$

where J_p is the incident proton current density, J_{sp} is the secondary electron current density produced by incident protons, J_e is the incident electron current density, J_{se} is the secondary electron current density produced by incident electrons, and J_{ph} is the photoelectron current density.

A charged surface at a given potential in a charged particle environment will accelerate particles of the opposite polarity and repel particles of the same polarity. Thus, assuming an omnidirectional Maxwellian energy distribution, the fraction of ambient plasma electrons reaching a large surface at a potential V is[10]

$$N_e = N_{e_o} \exp \left(\frac{eV}{K_{\tau_e}} \right) \quad , \quad V \leq 0 \tag{3}$$

where N_e is the incident electron density, N_{e_o} is the ambient electron density, V is the potential of the surface under consideration, K is Boltzmann's constant, e is the charge of an electron, and τ_e is the absolute temperature of the M-B electron energy distribution.

The average ambient electron current density incident to a neutral surface is given by

$$J_{e_o} = N_{e_o} e \bar{v}_e \tag{4}$$

where J_{e_o} is the average ambient electron current density and $\bar{v}_e$ is the mean ambient thermal velocity.

Thus, from Eqs. (3) and (4), the average electron current density incident to a large surface at potential V is

$$J_e = N_e \, e \, \bar{v}_e = J_{e_o} \left(\frac{eV}{K\tau_e} \right) \quad , \quad V \lesssim 0 \tag{5}$$

or

$$J_e = J_{e_o} e^{(V/T_e)} \quad , \quad V \leq 0 \tag{6}$$

where

$$T_e = \frac{K\tau_e}{e} \tag{7}$$

is the equivalent temperature, expressed in volts, of the M-B distribution approx-
imating the plasma electron energy distribution, and J_e is the electron current
density incident to a large surface at potential V. For a positive surface

$$J_e = J_{e_o} \quad , \quad V \geq 0 \tag{8}$$

That is, a surface at a positive potential will attract oppositely charged particles
but cannot extract more particles from the plasma environment than the ambient
particle density N_{e_o}. Similarly, the proton current density incident to a large
surface at potential V is

$$J_p = J_{p_o} e^{-V/T_p} \quad , \quad V \geq 0 \tag{9}$$

and

$$J_p = J_{p_o} \quad , \quad V \leq 0 \tag{10}$$

where J_{p_o} is the average ambient proton current density incident to a neutral sur-
face, and T_p is the equivalent temperature of the M-B distribution approximating
the plasma proton energy distribution and is expressed in volts.

In addition to the above charged particle fluxes, there will be secondary emis-
sion electrons as well as photoelectron emissions. Both types of charged particles
will be repelled by a surface at a negative potential and attracted by a surface at a
positive potential. Consequently, based on the previous discussion, the secondary
electrons leaving a surface of potential V is given by

$$J_{se} = J_{se_0} \, e^{-V/T_s} \quad , \quad V \geq 0 \tag{11}$$

$$J_{se} = J_{se_0} \quad , \quad V \leq 0 \tag{12}$$

$$J_{sp} = J_{sp_0} \, e^{-V/T_s} \quad , \quad V \geq 0 \tag{13}$$

$$J_{sp} = J_{sp_0} \quad , \quad V \leq 0 \tag{14}$$

where J_{se_0} and J_{sp_0} are the average secondary electron current densities emitted from a neutral surface produced by incident electrons and protons, respectively, J_{se} and J_{sp} are the secondary electron current densities emitted by the incident electrons and protons, respectively, and T_s is the equivalent temperature of the M-B distribution representing the energy distribution of the secondary emission electrons and is expressed in volts. The secondary emission electron current densities are directly related to the incident particle current densities. It is assumed that the secondary electrons emitted from a neutral surface are related to the incident particles by a fixed constant and can be expressed as

$$J_{se_0} = J_e \, f_e \tag{15}$$

$$J_{sp_0} = J_p \, f_p \tag{16}$$

where f_e is the ratio of secondary electrons to incident electrons and f_p is the ratio of secondary electrons to incident protons. In general, the secondary emission constants, f_e and f_p, will have different values for dielectric and metallic surfaces.

A similar development holds for the photoelectron emissions produced by sun illumination. The photoelectron current is directly proportional to the intensity of sunlight which is related to the angle of incidence. Consequently, the photo-electron current density emitted from a surface at potential V can be expressed as

$$J_{ph} = J_{ph_0} \, e^{-V/T_{ph}} \cos \alpha \quad , \quad V \geq 0 \tag{17}$$

244

$$J_{ph} = J_{ph_o} \cos \alpha \quad , \quad V \leq 0 \tag{18}$$

where J_{ph} is the photoelectron current density emitted from an illuminated surface at potential V, J_{ph_o} is the average photoelectron current density emitted from an illuminated neutral surface, T_{ph} is the equivalent temperature of the M-B distribution representing the energy distribution of the photoelectrons expressed in volts, α is the angle between the sun-line and the surface normal vector (sun/spacecraft surface aspect angle) and

$$\cos \alpha = \begin{cases} \cos \alpha \text{ for } |\alpha| < \pi/2 \\ \\ 0 \quad \text{for } |\alpha| \geq \pi/2 \quad \text{(self-shadowing conditions)} \quad . \end{cases} \tag{19}$$

The total positive current density into a surface can take one of four possible forms depending on the polarity, positive or negative, of the surface potential and the presence or absence of sun illumination. Thus, for a large dielectric surface, the current forcing function will have the general form

$$I_D(V) = \left[J_{p_o} e^{-V/T_p} \left(1 + f_{p_D} e^{-V/T_s} \right) + J_{ph_o} (\cos \alpha) e^{-V/T_{ph}} \right. $$
$$\left. + J_{e_o} e^{V/T_e} \left(f_{e_D} e^{-V/T_s} - 1 \right) \right] \cdot A \tag{20}$$

where I_D is the total positive current into a large dielectric surface, A is the area of the surface, and all other terms have been defined previously. The above equation must satisfy the following condition

$$e^{sV/X} = \begin{cases} 1 \text{ if } s = +1 \text{ and } V > 0; \text{ otherwise leave unchanged} \\ \\ 1 \text{ if } s = -1 \text{ and } V \leq 0; \text{ otherwise leave unchanged} \quad . \end{cases} \tag{21}$$

Exposed metallic parts of the structure can be located on many different outer surfaces of the spacecraft; consequently, the various exposed metallic surfaces, which are electrically connected, can have different sun-illumination conditions and the current forcing function will have a more complex form. In addition, the exposed metallic surfaces are generally small in area. Fewer charged particles will be deflected from a small surface at a given potential than a large surface at

245

the same potential; consequently, a correction factor must be applied to small surface areas. Thus, the positive current flowing into the exposed metallic structure is

$$I_M(V) = A_{M_T} J_{p_0} (1 + V/T_p) e^{-V/T_p} \left(1 + f_{p_M} e^{-V/T_s}\right)$$

$$+ A_{M_T} J_{e_0} e^{V/T_e} \left(f_{e_M} e^{-V/T_s} - 1\right)(1 + |V/T_e|)$$

$$+ \sum_{i=1}^{m} A_{M_i} J_{ph_0} (\cos \alpha_i) e^{-V/T} ph \tag{22}$$

where Eq. (21) holds for the above equation, A_{M_T} is the total exposed metallic area, A_{M_i} is the exposed area of the ith metallic surface, m is the total number of exposed metallic surfaces, α_i is the sun aspect angle for the ith metallic surface, and the following holds for the small area correction terms[7]

$$(1 + V/T_p) = \begin{cases} (1 + V/T_p) \text{ for } V \geq 0 \\ \\ 1 \text{ for } V < 0 \end{cases} \tag{23}$$

$$(1 + |V/T_e|) = \begin{cases} (1 + |V/T_e|) \text{ for } V \leq 0 \\ \\ 1 \text{ for } V > 0 \end{cases} \tag{24}$$

Equations (20) and (22) are the plasma and photoemission generated current sources and constitute the forcing functions of the spacecraft charging equations.

2.2 Material Properties and Configuration

The spacecraft outer surface material properties and configuration definition are needed to complete both the geometrical and electrical models. Essentially, the material properties and configuration definition consist of describing the location of the various outer surface thermal blankets and coatings and their electrical properties. The location of the materials is needed in the geometrical model to establish the number of constituent planar and curved surfaces of the spacecraft. The electrical properties of the materials are needed in the electrical model to determine the equivalent circuit element values of the outer surfaces of the spacecraft.

The electrical properties of the outer surface thermal materials that are most important in a spacecraft charging analysis are:

(1) The relative dielectric constant.

(2) The variation of the surface resistivity with respect to electrical stress level.

(3) The variation of bulk resistivity with respect to electrical stress level.

(4) Ratio of surface to bulk leakage currents.

All of the above properties can be determined experimentally. In fact, for meaningful results, the last three parameters should be measured under conditions similar to those experienced in the charged particle environment at synchronous orbit during a substorm. That is, the measurement results will be somewhat dependent on the energy levels and current densities of the charged particles bombarding the dielectric surface of the thermal blanket materials. In practice, however, these properties are measured by bombarding the materials with a monoergetic electron beam.

2.3 Geometrical Model.

The purpose of the geometrical model is to define the spacecraft outer surface areas in terms of approximate planar and curved surface projections, establish a reference coordinate system in the spacecraft, and define the vertices of all of the planar and curved surfaces in terms of the reference coordinate system. Furthermore, the results of the geometrical model are needed to complete the electrical model. That is, the approximate geometrical surfaces of the spacecraft outer configuration are used in the computation of the equivalent capacitor and resistor element values of the electrical model (each value is related to the surface area). The reference coordinate system can be selected anywhere inside the vehicle structure and should be chosen such that one or more coordinate axes are parallel to the axes of symmetry, or parallel to the major planar outer surfaces.

The reference coordinate system is useful in determining the relative locations and orientations of the constituent outer surfaces. In addition, the reference coordinate system is needed to determine the location of the spacecraft with respect to the earth and sun. The surface vertices are used in the computation of the surface normal vectors, and the surface normal vectors together with the location of the spacecraft with respect to the sun are used to determine the sun illumination condition of the surface; that is, whether the surface is illuminated by the sun, self-shadowed, or earth-shadowed. It should be noted that there can exist outer surfaces that are never illuminated by the sun; these areas are designated as "permanently" shadowed areas.

In order to determine the sun-illumination condition of the constituent surfaces, all outer surface areas must be expressed in terms of the six major planes parallel to the coordinate axes. Hence, the areas of the constituent planar surfaces parallel to a coordinate axis can be easily expressed in terms of the six major planes. However, for planar surfaces not parallel to a coordinate axis, the effective surface areas projected into the six major planes must be determined. The projected areas in the six major planes are then assumed to have the same normal vectors associated with the six major planes when determining their sun-illumination condition; however, the true, unprojected area is used when determining the area that is subject to the charged particle environment. The same procedure is followed for all curved surfaces, that is, cones, spheres, cylinders, etc.

The exposed metallic parts of the spacecraft structure require special attention. Since the exposed structural parts can exist on almost any constituent planar surface of the spacecraft, the exposed metallic parts will have different sun-illumination conditions depending on the particular location of the exposed part. The effective projected area of each exposed metallic part is computed in each of the six major reference planes as outlined above. The effective projected area in conjunction with the particular sun/spacecraft surface aspect angle is used in the computation of the photoemission current; this is represented by the last term of Eq. (22). However, the actual exposed area of a metallic part is subject to the plasma environment; thus, the total exposed metallic area is used in the computation of the incident particle currents. This is represented by the first two terms of Eq. (22).

2.1 Electrical Model

The electrical model defines the lumped element, equivalent circuit representation of the spacecraft outer surfaces with respect to the electrostatic charging phenomenon. The equivalent electrostatic circuit is a network consisting of capacitors and resistors whose values are either computed or measured. It will be assumed that a dielectric surface can be represented as a simple lumped capacitor and a parallel leakage resistance; however, this is an approximate representation when considering the complex processes that occur when a dielectric surface is bombarded by high energy particles. The capacitor components represent the capacitance of the various dielectric surfaces with respect to the spacecraft structure. The resistor components represent the leakage current from the dielectric surfaces to the spacecraft structure. Additional capacitors and resistors are needed to represent the surface capacitance and leakage current between adjacent surfaces and between illuminated and nonilluminated sections of a surface. However, these surface interaction processes are second-order coupling effects and will not be considered in the model. This is a conservative assumption and does

not affect the ability of the model to predict the potential differences between a surface and the structure or the potential differences between adjacent surfaces. Consequently, the equivalent circuit of the spacecraft with respect to the charging phenomenon has the simplified form shown in Figure 2.
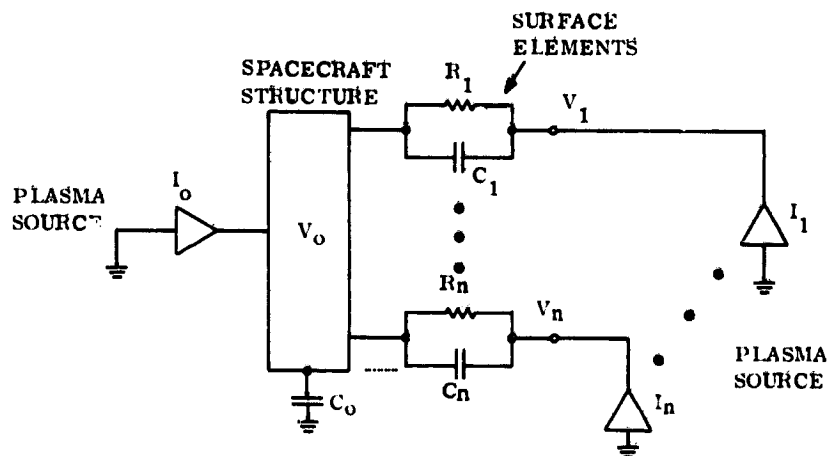

Figure 2. Spacecraft Equivalent Circuit

It has been assumed that there are n outer surfaces. The i-th surface has an absolute potential of V_i volts and each surface, or node, has a corresponding plasma and photoemission generated current source having the general form of Eq. (20). The spacecraft structure has an absolute potential of V_o volts and I_o is the plasma and photoemission generated current source into the exposed metallic surfaces and is given by Eq. (22). The capacitance, C_o, is the intrinsic capacitance of the spacecraft structure with respect to the plasma. This structural capacitance can be approximated by the isolated capacitance of the structure. This is a reasonable approximation since the plasma sheath outer boundary, which represents the terminus of the strong satellite fields due to spacecraft charging, has a depth on the order of tens of meters.

249

The following set of simultaneous spacecraft charging equations can be written for the simplified circuit of Figure 2:

$$\frac{C_1 \, d \, (V_1 - V_o)}{dt} + \frac{(V_1 - V_o)}{R_1(V_1 - V_o)} = I_1(V_1)$$

$$\vdots \qquad\qquad \vdots \qquad\qquad \vdots$$

$$\frac{C_n \, d \, (V_n - V_o)}{dt} + \frac{(V_n - V_o)}{R_n(V_n - V_o)} = I_n(V_n)$$

$$C_o \frac{dV_o}{dt} = \sum_{i=0}^{n} I_i \tag{25}$$

Equation (25) in general will be nonlinear since the leakage resistances are non-linear functions of stress level $(V_i - V_o)$ and the plasma and photoemission generated currents are nonlinear functions of absolute potential. The number of equations, n, is a function of both the number of surfaces with different dielectric materials and the number of surfaces with different sun-illumination conditions.

2.5 Solar/Earth/Spacecraft Orbit Model

The purpose of the solar/earth/spacecraft orbit model is to determine the sun-illumination condition of a spacecraft surface including both earth-shadowing and self-shadowing conditions. The sun-illumination condition of a surface is determined by first defining the planar surface and its vertices with respect to the spacecraft reference coordinate system. This is essentially accomplished in the geometrical model. Next, the normal vector of this surface is computed and the relative location of the normal vector with respect to the spacecraft reference coordinate system is determined. The relative position of the sun with respect to the earth is computed as well as the relative position of the spacecraft with respect to the earth. Using coordinate transformations, the relative position of the space-craft coordinate system with respect to the sun is then determined. Finally, the angle between the surface normal and the sun vector, the aspect angle, is com-puted. The intensity of sun-illumination is proportional to the cosine of the aspect angle with full illumination occurring for an aspect angle of 0°. The surface is self-shadowed when the absolute value of the aspect angle exceeds 90°. Also, the earth-shadowing condition, which occurs when the spacecraft is in the umbra of the earth, can be similarly determined. The solar/earth/spacecraft orbit

250

model consists of four separate parts: the spacecraft ephemeris model, the solar model, the coordinate transformations, and the solar/vehicle/earth geometrical model.

The relative geometry between the earth, the sun, the spacecraft, and a constituent surface is shown in Figure 3. As indicated in Figure 3, the surface is defined by the vertices A, B, and C. To determine the solar/spacecraft surface aspect angle, the surface normal vector and the surface-sun vector must be computed. The vertex vectors of the surface expressed in vehicle coordinates are

$$\left. \begin{array}{c} \overline{FA} \\ \overline{FB} \\ \overline{FC} \end{array} \right\} \tag{26}$$

and the sun vector in inertial coordinates at the center of the earth is

$$\overline{OS} \tag{27}$$

and is computed by the solar model program. The spacecraft vector expressed in inertial coordinates is

$$\overline{OF} \tag{28}$$

and is computed by the vehicle ephemeris program.

From Figure 3, it can be seen that the surface normal vector is given by

$$N = (\overline{FA} - \overline{FB}) \times (\overline{FC} - \overline{FB}) \tag{29}$$

the solar/spacecraft surface aspect angle is then given by

$$\cos \alpha = (\overline{N} \cdot \overline{BS})/(|\overline{N}| \, |\overline{BS}|) \quad , \tag{30}$$

and the earth aspect angle is

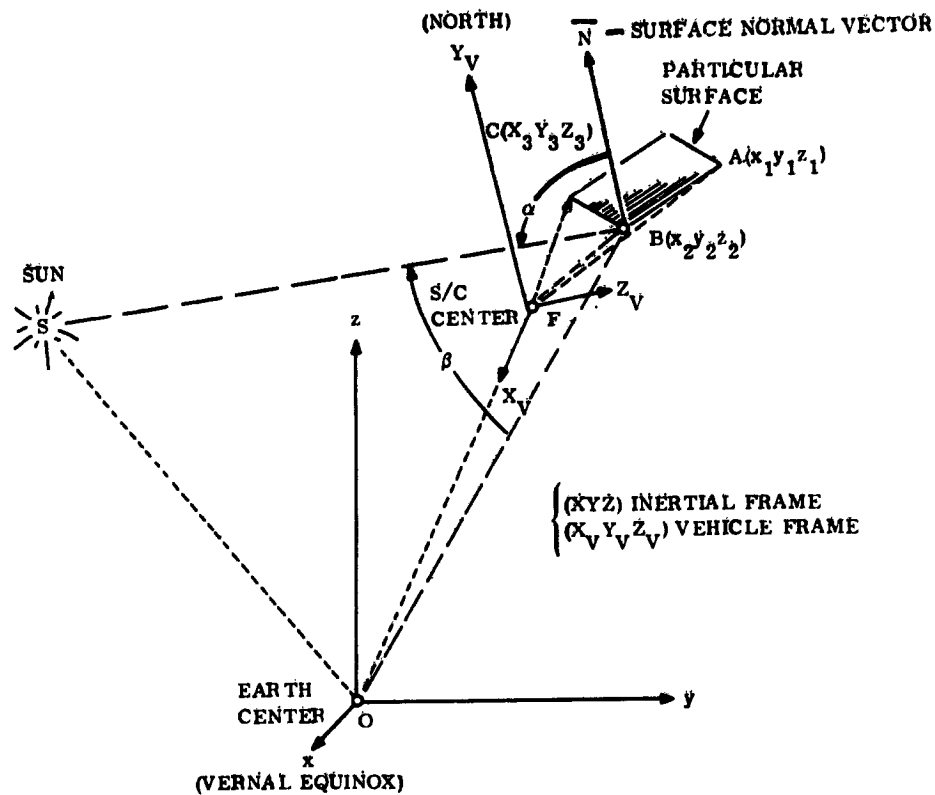$$\cos \beta = (\overline{BS} - \overline{BO})/(|\overline{BS}| \, |\overline{BO}|) \quad . \tag{31}$$

Figure 3. Sun-Earth-Spacecraft Orbital Geometry

Earth-eclipsing (shadowing) of a surface is given by the following condition

$\beta < \beta_T$ eclipse condition

$\beta \geq \beta_T$ non-eclipse condition

(32)

where

$$\beta_T = \sin^{-1} (R_e/r)$$
$$R_e = \text{radius of earth}$$
$$r = |\overline{OF}|$$

(33)

and β_T is the earth disc aspect angle subtended at the spacecraft. Thus, an earth-eclipsing condition occurs when the spacecraft is in the umbra of the earth. Self-shadowing or self-eclipsing of a surface by the spacecraft itself is given by the following condition:

252

$$|\alpha| \geq \pi/2 \quad \text{eclipse condition}$$

$$|\alpha| < \pi/2 \quad \text{non-eclipse condition}$$

(34)

where α is the solar/spacecraft surface aspect angle determined from the solar projection upon the surface normals.

In the simplified spacecraft ephemeris model, the location of the spacecraft with respect to the inertial coordinate system of the earth is determined. There is no need for a precise spacecraft orbit so an abbreviated model is used. The orbit is assumed to be circular with a constant radius and a nominal period of 1440 min. The spacecraft is flown in the equatorial plane (inclination $= 0^{\circ}$). In the solar model, the position of the sun with respect to the earth is derived from the American Ephemeris and Nautical Almanac which provides mean position in terms of a series expansion of elapsed centuries from a base epoch. Conventional coordinate transformations are employed to determine the position of the sun with respect to the spacecraft (vehicle) reference coordinate system.

2.6 Numerical Integration Approach

The first order, simultaneous, nonlinear spacecraft charging differential Eqs. (25) with forcing functions represented by Eqs. (20) and (22) are of such a form that standard closed-form methods of solution do not apply. Consequently, several "initial value" numerical integration techniques were utilized to compute the time response of the absolute potentials, $V_1, \ldots, V_n$. The greatest success was achieved with the Runge-Kutta[11] integration process. After some preliminary experimentation, it was found that a step size of 0.001 sec produced satisfactory results in the time response computation. The step size is the incremental value of the independent variable, time, at which the dependent variable value, absolute potential, is computed.

From initial computations of the time response of the set of Eqs. (25) using actual circuit values of capacitance and nonlinear resistance and actual plasma substorm parameters, it became apparent that the transient and steady-state results could not be obtained in a single numerical integration execution. First, it was found that the steady-state values of potential are reached after several hours. Second, the computer execution time-to-solution time was enormous (typical run times were on the order of 20 to 30 min to obtain 1 to 3 min of simulated time). Consequently, it was decided to characterize the transient behavior by computing the transient response up to that point in time at which the transient response was well-behaved, that is, either monotonically decreasing or increasing (usually on the order of 1 to 3 min). The steady-state solution was computed

separately in a rapidly executed program. This overall approach was not rigorously accurate since plasma conditions can change within minutes and illumination conditions can change within tens of minutes. However, if worst case plasma and illumination conditions are employed, the solutions, both transient and steady-state, will represent worst case values and more accurate solutions should not be necessary.

To obtain the steady-state solution, a more direct method was employed. The steady-state condition is characterized by the condition $dV_i/dt = 0$. From Eq. (25), this results in the steady-state system of equations

$$\frac{dV_i}{dt} = 0 = \frac{1}{C_i} \left[I_i - \frac{(V_i - V_o)}{(R_i(V_i - V_o))} \right] \quad , \quad 1 \le i \le n \tag{35}$$

and

$$\frac{dV_o}{dt} = 0 = \sum_{i=0}^{n} I_i \quad . \tag{36}$$

The solution to this system of equations can be viewed as an optimization problem where Eq. (36), which represents the current balance condition, must be minimized while simultaneously satisfying the set of n nonlinear equations, Eqs. (35), which can be considered as constraint equations on the current balance condition. For simplicity, it was decided to use a simple direct enumeration scheme to iteratively search the region

$$V_L \le V_i \le V_U \quad , \quad 0 \le i \le n \tag{37}$$

where

$$V_i = V_L + n\Delta V \quad , \quad 0 \le i \le n \tag{38}$$

such that Eq. (36) was minimized while satisfying the n constraint Eqs. (35). The terms V_L and V_U are the lower and upper bounds, respectively, of the absolute potentials of the surfaces and structure. Positive potential values were incremented by $\Delta V = 0.1$ volts and negative potential values by $\Delta V = 50$ volts.

254

3. SPACECRAFT CHARGING SIMULATION RESULTS

Spacecraft charging simulation results for a three-axis stabilized spacecraft
are presented in this section. The spacecraft analyzed, with thermal blankets in
place, could be adequately modeled geometrically as a "box-like" structure with
large "flat panel" type solar cell arrays which are located above and below the
north and south panels, respectively, of the main spacecraft structure. The
antenna structures, with thermal blankets, could be modeled as conical structures
that protrude from the front side of the spacecraft main structure and point towards
the earth's surface. The dielectric properties of the thermal blankets and surface
coating materials were measured and the equivalent capacitances and leakage
resistances of the constituent surfaces were computed. The results are listed in
Table 1. There were 13 surfaces with either different materials or different
orientations (with respect to the spacecraft reference coordinate system) that had
to be considered in the spacecraft charging analysis. The front side had three
different materials and the north and south panels had two different materials.
The resistor values listed in Table 1 are based on the bulk resistivity character-
istic and represent the values computed at low stress level. The last element in
the table is the structural capacitance and was computed by using some of the
formulas listed in Appendix A.

Table 1. Element Value Summary of Three-Axis Stabilized Spacecraft
Analyzed

Element Location	Resistor Value (ohms)	Capacitor Value (μf)
1. Backside	$R_1 = 8.9 \times 10^7$	$C_1 = 0.37$
2. West Panel	$R_2 = 1.2 \times 10^8$	$C_2 = 0.29$
3. North Panel	$R_3 = 2.1 \times 10^8$	$C_3 = 0.16$
4. North Panel	$R_4 = 1.8 \times 10^9$	$C_4 = 0.16$
5. South Panel	$R_5 = 1.4 \times 10^8$	$C_5 = 0.24$
6. South Panel	$R_6 = 4.0 \times 10^{10}$	$C_6 = 0.08$
7. East Panel	$R_7 = 1.2 \times 10^8$	$C_7 = 0.28$
8. Front Panel	$R_8 = 2.5 \times 10^8$	$C_8 = 0.13$
9. Front Side	$R_9 = 9.5 \times 10^{10}$	$C_9 = 0.069$
10. Front Side	$R_{10} = 2.8 \times 10^{11}$	$C_{10} = 0.024$
11. Solar Array Sun-Side	$R_{11} = 3.0 \times 10^{10}$	$C_{11} = 0.65$
12. Solar Array Dark-Side	$R_{12} = 1.4 \times 10^8$	$C_{12} = 4.4$
13. Permanently Shadowed Sides	$R_{13} = 3.8 \times 10^8$	$C_{13} = 0.087$
14. Spacecraft Structure	------	$C_{14} = 0.000356$

In general, the bulk resistivity is a function of stress level. The bulk resistivities of all the dielectric materials were measured by bombarding samples of the materials by high energy electrons and measuring the through conduction leakage current as a function of electron accelerating beam voltage. It was conservatively assumed that the surface stress level was approximately equal to the beam voltage and a piecewise approximation to the bulk resistivity versus beam voltage characteristic was computed. All of the piecewise approximations of the dielectric materials had a form similar to the piecewise approximation of Chemglaze paint shown in Figure 4. To simplify the simulation and to decrease the execution time, the piecewise approximation of all of the materials were employed in the analysis.
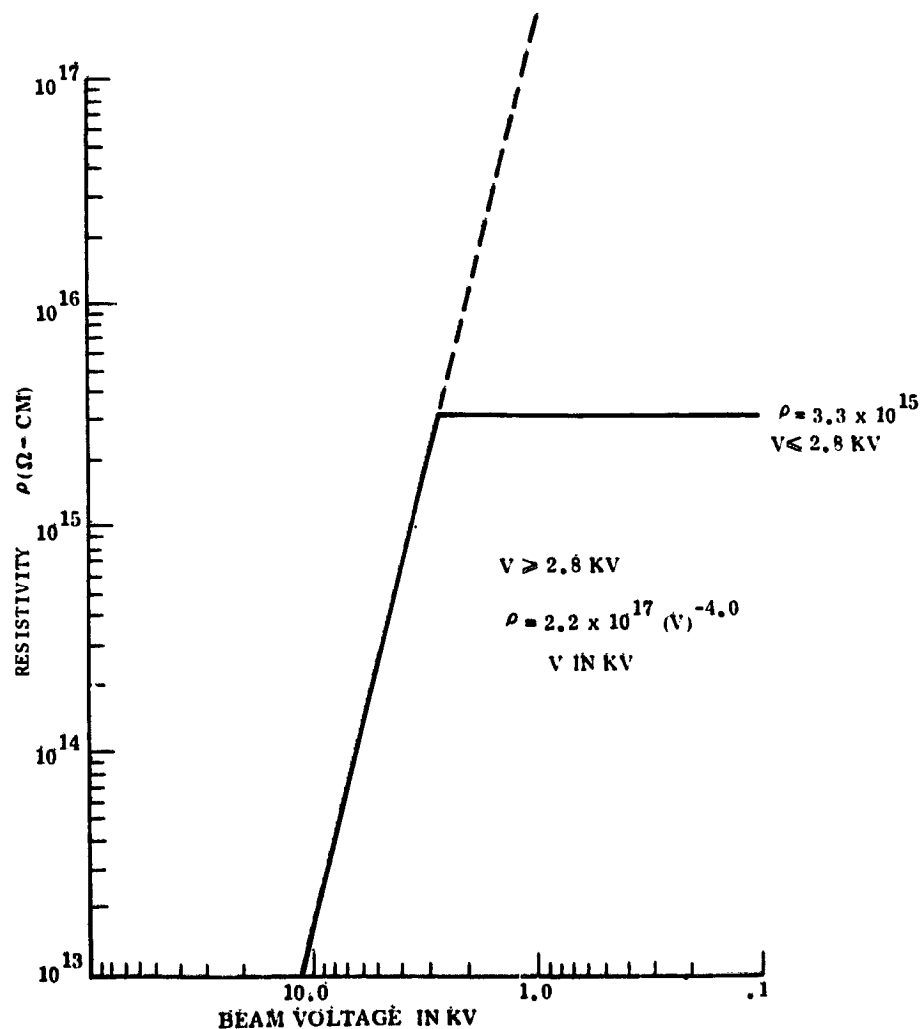

Figure 4. Piece-Wise Approximation of Chemglaze Paint Bulk Resistivity

256

Spacecraft charging simulation results were obtained for the three-axis stabilized spacecraft during the peaks of the fall-equinox and winter-solstice periods. These two periods of the earth-sun orbit represent the extremes of sun-illumination condition experienced by a geosynchronous satellite. For example, during the equinox period the satellite is totally shadowed because of earth-eclipsing and the spacecraft structural potential will achieve its highest-negative value. The earth eclipse period can last as long as 72 min roughly from 23:30 to 0:45 local time. During the peak of the winter-solstice period the south panel of the spacecraft as well as the solar array, east panel, and backside are sun-illuminated. The maximum amount of exposed metal that is illuminated by the sun occurs during this period because the south panel has more exposed metal than the north panel; if the reverse had been true, the maximum amount of exposed metal that is illuminated by the sun would occur during the summer-solstice period. Thus, during the winter-solstice period the spacecraft structure will achieve it lowest negative value.

Using the average plasma substorm parameters of the 2 January 1970 substorm, which was the worst substorm measured by ATS-5 during the first 50 days of 1970, and assuming a time-invariant, omnidirectional charged particle substorm, the absolute potentials of the spacecraft structure and outer surfaces were computed. That is, it was assumed in the analysis that the substorm can be adequately represented as a "step" function in electron and proton temperatures and particle current densities over their values that normally occur during the "quite-time," that is, their quiescent conditions.

The average substorm parameters as well as other parameters used in the analysis are listed in Table 2. The complete substorm profiles for the 2 January substorm as well as the average values have been given in a previous paper. [6] Based on ATS-5 data of the 2 January substorm, a "step" function of 9 hr duration was employed in the simulation model, existing roughly from 23:00 to 8:00 local time. Starting with initial values of zero absolute potential at 23:00 hours, the Runge-Kutta numerical integration procedure was employed to determine the variation of the surface and structural potentials with time. Since the numerical integration technique produced roughly 60 sec of simulation results for every 1000 sec of execution time, the continuous substorm response could not be computed for the full 9 hr duration. Instead, the transient solution was computed using the Runge-Kutta procedure until the surface and structural potential time responses were well-behaved and approaching their steady-state values.

Since the magnitude of the transient response is approximately proportional to the magnitude of the change in forcing function conditions, the more significant transient responses will occur when there is a significant change in the particle

Table 2. Photoemission, Secondary Emission, and Omnidirectional Plasma Parameters

Parameter	Typical Range	Value Selected
T_{ph}	$1\ V \leq T_{ph} \leq 3\ V$	2 V
T_s	$2\ V \leq T_s \leq 4\ V$	2 V
f_{e_M}	$0 \leq f_{e_M} \leq 1$	0.5
f_{e_D}	$0 \leq f_{e_D} \leq 1$	0.75
f_{p_M}	$0 \leq f_{p_M} \leq 1$	0.5
f_{p_D}	$0 \leq f_{p_D} \leq 1$	0.75
T_e	----	6.0 kV (substorm) 3.0 kV (quiet) 20.0 kV (severe substorm)
T_p	----	12.0 kV (substorm) 6.0 kV (quiet) 40.0 kV (severe substorm)
J_{ph_o}	$0.82\ na/cm^2 \leq J_{ph_o} \leq 4\ na/cm^2$	$2.0\ na/cm^2$
J_{e_o}	$0.02\ na/cm^2 \leq J_{e_o} \leq 2\ na/cm^2$	$0.6\ na/cm^2$ (substorm) $0.02\ na/cm^2$ (quiet)
J_{p_o}	$2\ pa/cm^2 \leq J_{p_o} \leq 32\ pa/cm^2$	$0.02\ na/cm^2$ (substorm) $2.0\ pa/cm^2$ (quiet)

current densities or energies. Consequently, transient solutions were obtained at the onset of the plasma substorm, where particle temperatures (energies) and current densities change suddenly from their quiescent values to their substorm values; at the beginning of earth-eclipse, where the photoelectron current forcing function is zero; and at the end of earth-eclipse, where the photoelectron current forcing function becomes nonzero. The transient response of the structure, the solar array, and the surface that exhibited the greatest steady-state potential difference is shown in Figure 5 for the onset of the 6 kV substorm. In this figure, as well as the others to be presented, the transient response is shown for a period of 70 sec and the steady-state solutions are shown on the right side of the figure. The transition period from the transient to the steady-state solutions is indicated by the dashed lines. (As expected, the surface that consistently exhibited the
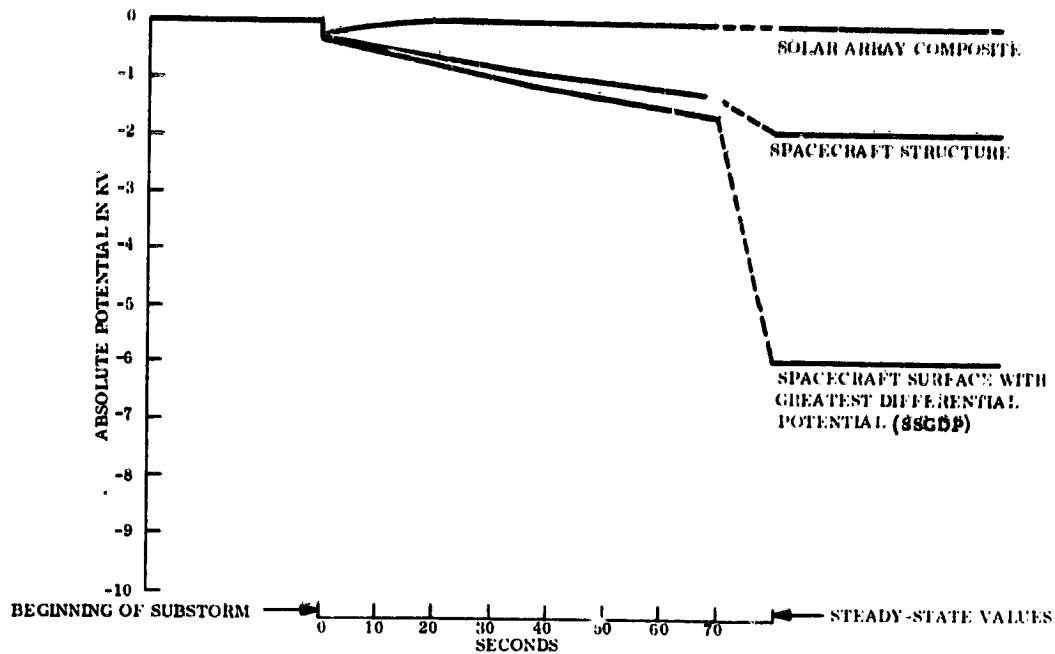
258

Figure 5. Transient Response at Onset of a 6 kV Substorm. Fall-Equinox 23:00 LT

greatest steady-state potential difference between the structure and the surface itself, was covered with dielectric material that experimentally had the highest value of bulk resistivity.) It was assumed that all potentials were initially at zero volts. It can be seen that the surfaces "fall" instantaneously to a few hundred volts with small potential differences between the two outer surfaces and the underlying structure. This behavior was typical of all of the surfaces of the spacecraft. The absolute potentials than "fall" monotonically negative until, after a long period of time, the final steady-state values are achieved. The transient response at the onset of earth-eclipse is shown in Figure 6. It was assumed, as a worst case, that the steady-state values of the previous period had been achieved at the start of the earth-eclipse and are the initial values used in the numerical integration program. It can be seen that the structure instantaneously "falls" to a negative value of about 9 kV, however, the initial potential differences are maintained but decrease monotonically in the steady-state to small values on the order of a few hundred volts. The transient response at the end of the earth-eclipse period is shown in Figure 7. Again it was assumed, as a worst case, that the steady-state values of the previous period had been achieved at the end of the earth-eclipse period and these values then became the initial values in the numerical integration program. The structural potential instantaneously decreases to a negative value of
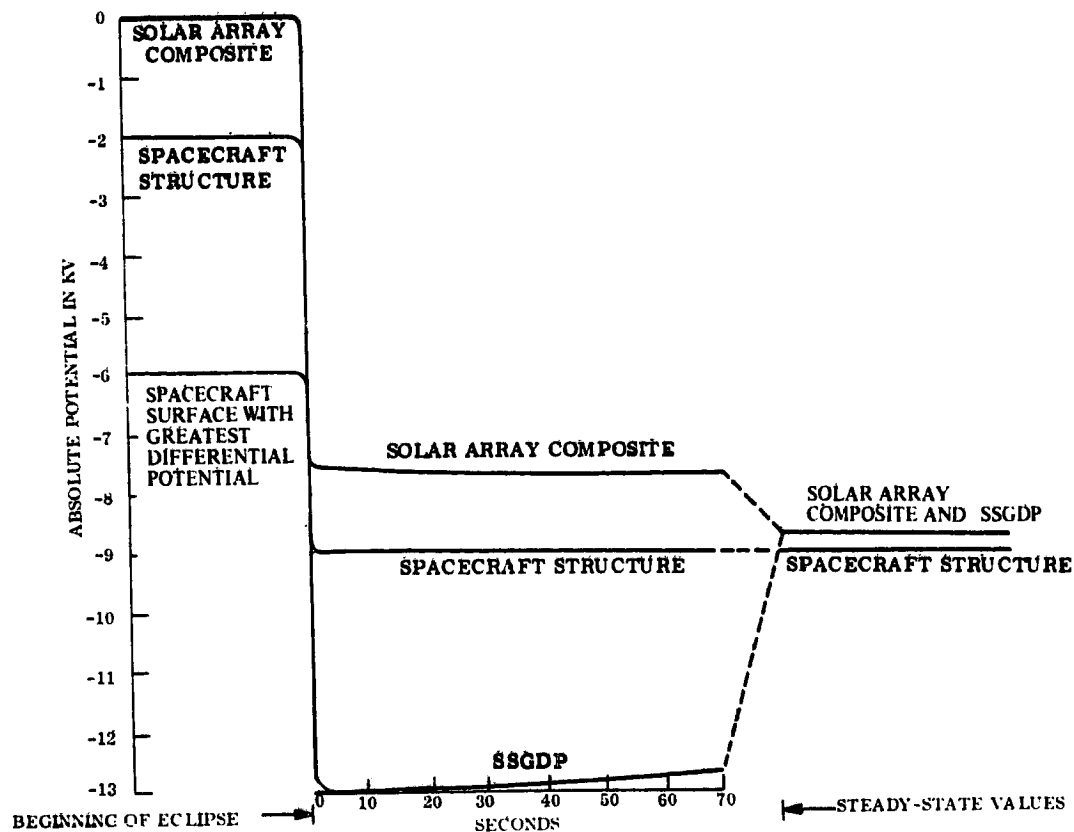
259

Figure 6. Transient Response into Eclipse for a 6 kV Substorm. Fall-Equinox 23:30 LT

a few hundred volts; however, the potential differences are maintained initially and then increase monotonically to somewhat larger values. The solar array is "clamped" to zero volts (actually less than one volt positive) by photoemission. This condition occurs for most surfaces with full sun-illumination intensity.

Upon comparing the steady-state with the transient solution values, it becomes apparent that the final steady-state values, that is, those values achieved if the sun-illumination conditions did not change, represent the worst-case differential values. Also, the differential potentials can change instantaneously by no more than a few hundred volts. But, the absolute potential of the spacecraft structure
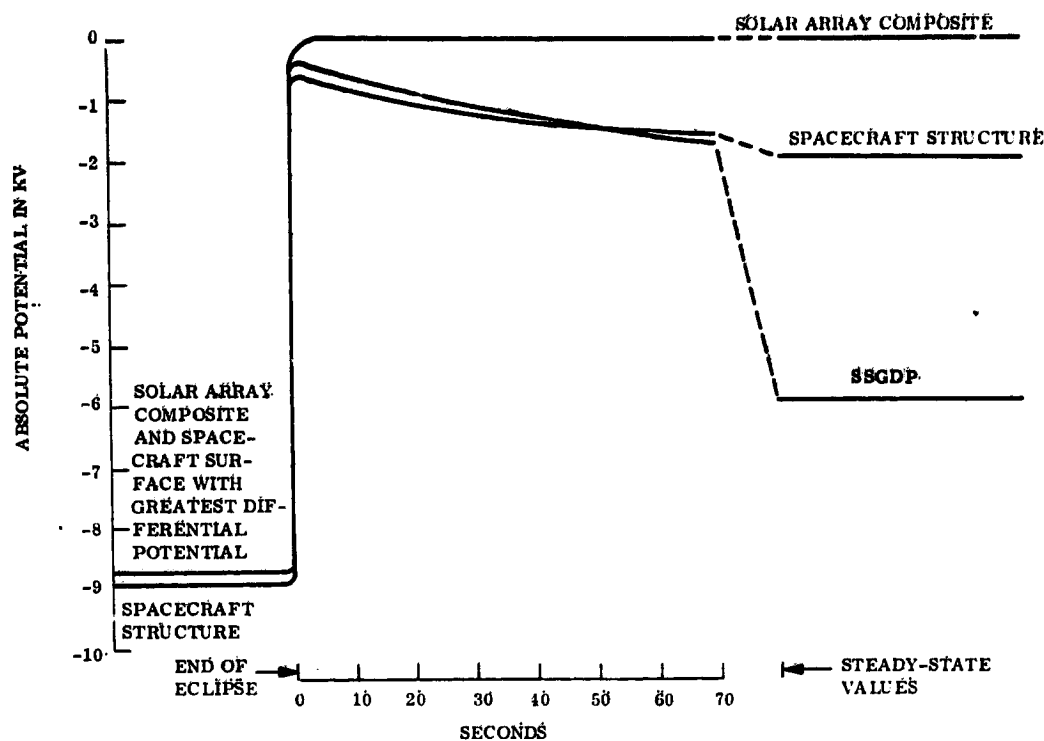
260

Figure 7. Transient Response Out of Eclipse for a 6 kV Substorm. Fall-Equinox 00:45 LT

can change almost instantaneously since it has small capacitance. In all cases, the transient response times are controlled by either the potential constants of the forcing functions or the time constants of the circuit elements or both. The differential potentials of the outer surfaces do not change instantaneously by large amounts since the circuit element time constants, which are large in value (the product of resistance and capacitance), are dominant. However, the absolute potential of the surfaces, which is the sum of the absolute potential of the structure and the differential potential between the surface and the structure, can change instantaneously in conjunction with the structure. This is demonstrated in all of the transient responses and in particular in Figures 6 and 7. At the beginning and at the end of earth-eclipse, the absolute potential of the structure changes by a large amount and the absolute potentials of the surfaces change by a similar amount; thus the potential differences do not change in value initially.

At the onset of the substorm, the structure "falls" slowly negatively since there are photoelectron emissions which tend to cancel the influx of electrons from the plasma current source. At the onset of earth-eclipse there are no photoelectron currents and the plasma electron current sources dominant and rapidly charge-up the small structural capacitance. At the end of earth-eclipse, the large photoelectron current sources again reoccur. The large outflux of electrons from the exposed metallic parts produced by the photoemission currents is instantaneously supplied by the structural capacitance and consequently, there is a rapid decrease in the negative absolute potential of the structure.

As discussed previously, for three-axis stabilized spacecraft there is considerable diurnal as well as seasonal variations in the amount and location of the outer surface areas of the spacecraft that are exposed to the sun. Thus, the sun illumination condition of the 13 dielectric surfaces of the spacecraft are computed throughout the orbital path. From the solar/earth/spacecraft orbit model it was found that the sun-illumination condition did not change significantly in local time increments less than 30 min. Consequently, steady-state solutions were computed at 30 min increments throughout the duration of the substorm. In general, the final steady-state solution will never be achieved at the end of the 30 min period since some of the source potential and network time constants involved are on the order of thousands of seconds and the initial sun-illumination conditions, on which the final steady-state solution is based, will change significantly every 30 min. A summary of the spacecraft steady-state values using the average plasma parameter values of the 2 January substorm, is listed in Table 3 for 1 hr increments throughout the duration of the substorm for the fall-equinox period. The hourly incremental values are representative of the worst-case potential differences obtained when compared against the values computed in the smaller half-hour increments. The widely varying values of the absolute potential of the spacecraft structure are shown as well as the maximum surface differential potentials. It can be seen that during eclipse (lasting roughly from 23:30 to 0:45) the spacecraft, in steady-state, achieves a negative potential of about 9 kV and a maximum surface potential difference of -4.5 kV was reached towards dawn.

A similar analysis was conducted for the peak of the winter-solstice period for the 6 kV test substorm. As expected, the lowest negative spacecraft structural potential was achieved during this period. A summary of steady-state values is presented in Table 4. A maximum potential difference of -4.6 kV was achieved.

As can se seen from the summary tables, the spacecraft structural potential varies widely reaching a maximum negative value of about 9 kV at eclipse and a minimum negative value of 450 kV during the winter-solstice period. In this particular design, the structural exposed metal was kept to a minimum and this

262

Table 3. Summary of Steady-State Results for 6 kV Substorm During Fall-Equinox

Local Time	Material with the Maximum Potential Difference for Assumed Plasma Conditions		Absolute Potential of S/C Structure (volts)
	Absolute Potential (volts)	ΔV Between Surface and S/C Structure	
23:00	-5950	-4000	-1950
24:00 (eclipse)	-8750	200	-8950
1:00	-5950	-4000	-1950
2:00	-5500	-4250	-1250
3:00	-5500	-4250	-1250
4:00	-5500	-4250	-1250
5:00	-5700	-4200	-1500
6:00	-5850	-4050	-1800
7:00	-5350	-4350	-1000
8:00	-5200	-4500	-700

Table 4. Summary of Steady-State Results for 6 kV Substorm During Winter-Solstice

Local Time	Material with the Maximum Potential Difference for Assumed Plasma Conditions		Absolute Potential of S/C Structure (volts)
	Absolute Potential (volts)	ΔV Between Surface and S/C Structure	
23:00	-5250	-4400	-850
24:00	-5700	-4100	-1600
1:00	-5250	-4400	-850
2:00	-5200	-4500	-700
3:00	-5200	-4500	-700
4:00	-5200	-4500	-700
5:00	-5200	-4500	-700
6:00	-5350	-4350	-1000
7:00	-5050	-4600	-450
8:00	-5050	-4600	-450

helps to explain the fact that the structure never achieved zero potential when various exposed parts were illuminated by the sun. Examination of the steady-state values of all of the surfaces indicates that during eclipse all of the surfaces achieve almost the same absolute potential. This results from the fact that all surfaces have the same shadow and plasma current source conditions.

4. CONCLUSIONS AND DISCUSSION

This paper has been concerned with the development and application of a charging model for three-axis stabilized spacecraft. The objective of the model is to determine the differential potentials between the outer surfaces and the structure of a spacecraft throughout its geosynchronous orbit when under the influence of a geomagnetic substorm. It was assumed that the interaction between the plasma and the spacecraft can be adequately represented by an equilibrium theory approach. That is, the energy distribution of the constituent plasma particles can be expressed in terms of an omnidirectional Maxwell-Boltzmann distribution. The plasma is then represented by equivalent voltage dependent current sources and the outer surfaces by simple lumped elements. The resulting first order differential equations are integrated and potential distributions determined. Sun-illumination conditions were determined by a solar/earth/spacecraft orbit model and the intrinsic capacitance of the spacecraft with respect to the plasma sheath is approximated by its isolated capacitance. Spacecraft charging simulation results, including both the transient and steady-state solutions, have been presented.

A knowledge of the potential distribution of the outer surfaces and structure of the spacecraft throughout its orbital path is important from a systems design and analysis viewpoint. In general, spacecraft materials that maintain stress levels below their dielectric strength level should be selected. If, from the analysis, it appears that the dielectric strength of various spacecraft surface materials will be exceeded, then, depending on the magnitude and repetition rate of the discharge and location of the material, corrective action such as modification or replacement of the material may be necessary. Thus, the spacecraft charging simulation results can be useful in determining the selection and location of the type of outer surface thermal blanket or coating materials to be employed in the design of spacecraft.

The spacecraft charging simulation results can be useful in establishing the relationship between the amount and location of the exposed structural metallic parts and the absolute potential of the spacecraft structure. For example, from the spacecraft charging simulation results, it was found that when a maximum amount of exposed metal was illuminated by the sun, the structural potential achieved its lowest negative value (because of photoemission). At the same time, the surface differential potential attained its maximum value. Conversely, when a minimum amount of exposed metal was illuminated, the spacecraft structure achieved its highest negative value and the surface differential potential attained its minimum value. The above results demonstrate that it is desirable to employ design approaches that allow the structural potential to attain values between the surfaces "clamped" at zero potential and those with the highest negative potential since the differential potentials are than minimized. The exact design approaches taken will depend on the spacecraft configuration, orbit, and outer surface materials.

In the simulation analysis employing a step function, that is, time-independent, representation for the plasma substorm, the worst case differential potentials occurred at steady-state and not during the transient response. This representation is not realistic since the particle energies and current densities are slowly but widely varying functions of time. Because of the large time constants of the equivalent spacecraft circuit, a steady-state response using the actual time-dependent plasma forcing functions would never be reached. However, the transient response obtained with a step forcing function is indicative of the type of response that can be expected when using the time-dependent forcing functions. In addition, the steady-state response to a step forcing function can be used as an upper bound of the worst-case differential potentials when the step function is used with worst-case plasma values. This is supported by simulation results which indicate that the magnitude of the differential potentials as well as the absolute potentials are directly related to the magnitude of the substorm particle energies (temperatures) and current densities.

Upon examining the spacecraft charging results, it becomes apparent that the absolute potentials of the surfaces are controlled by the absolute potential of the structure. The structural potential can change instantaneously because of its small intrinsic capacitance. However, the time response of the differential potentials is controlled by the large time constants of the equivalent spacecraft electrostatic circuit and the large potential constants of the forcing functions.

The model presented in this paper is based on an equilibrium theory approach. Other, more accurate, but complex approaches take into consideration particles trajectories, their actual energy distributions, and determine the surface

potentials by solving Poisson's potential distribution equation in three dimensions. Although the model is based on simplistic assumptions, the simulation results obtained for the structural potential are in relative agreement with the structural potentials measured on-board ATS-6, a three-axis stabilized spacecraft. The charging model predicts that upon entering eclipse, the spacecraft structure falls almost instantaneously to a value of about -9 kV and leaving eclipse the spacecraft structure rises almost instantaneously to a few hundred volts negative. Similar transient results into and out of eclipse have been observed on ATS-6. In addition, the structural potential variations during the post-eclipse period, as predicted by the model, correspond, relatively, to measured results on ATS-6. For example, examining the steady-state stress levels in the post-eclipse period, it can be seen that the structural potential rises to a low negative value after eclipse but falls negatively towards dawn and then rises to a low negative value at dawn. These results are in relative agreement with data measured on board ATS-6.

References

1. DeForest, S. E. (1973) Electrostatic potentials developed by ATS-5, Photon and Particle Interaction with Surfaces in Space, R.J.L. Grard, Editor, D. Reidel Publishing Co., Dordrecht-Holland.

2. Inoye, G. T. et al (1975) Final Report, Spacecraft charging analysis: studies and analysis of the modified DSCS-II Flights 5 and 6 configuration, TRW Report.

3. Rosen, A. (1975) Spacecraft charging: Environment induced anomalies, AIAA 13th Aerospace Sciences Meeting, Pasadena, Calif., paper no. 75-91.

4. DeForest, S. E. (1972) Spacecraft charging at synchronous orbit, J. Geophys. Res. 77:651-659.

5. McPherson, D.A., Cauffman, D.P., and Schober, W. (1975) Spacecraft charging at high altitudes - The Scatha satellite program, AIAA 13th Aerospace Sciences Meeting, Pasadena, Calif. paper no. 75-92.

6. Inoye, G. T. (1975) Spacecraft charging model, AIAA 13th Aerospace Sciences Meeting, Pasadena, Calif. 1975, paper no. 75-255.

7. Inoye, G. T. et al (1974) Final Report, Spacecraft charging analysis: A study and analysis of the DSCS-II spacecraft orbital charging phenomena, TRW Report.

8. Fredricks, R.W., and Scarf, F.L. (1973) Observations of spacecraft charging effects in energetic plasma regions, Photon and Particle Interactions with Surfaces in Space, R.J.L. Grard, Editor, D. Reidel Publishing Co., Dordrecht-Holland.

9. DeForest, S. E., and McIlwain, C. E. (1971) Plasma clouds in the magnetosphere, J. Geophys. Res. 76(No. 3587).

10. Reitz, J.R., and Milford, F.J. (1960) _Foundations of Electromagnetic Theory_, Addison-Wesley Co., Reading, Mass.

11. Hamming, R.W. (1962) _Numerical Methods for Scientists and Engineers_, McGraw-Hill Co., New York, N.Y.

Electrostatic Capacitance of Several Isolated, Three-Dimensional, Geometrical Structures

I. INTRODUCTION

In this appendix, equations for the isolated electrostatic capacitance of several types of geometrical structures are given.

1.1 Sphere

The isolated capacitance of a sphere is[1]

$$C_{ISO} = 4\pi\varepsilon_o R \tag{A1}$$

where C_{ISO} is expressed in farads, R is the radius of the sphere in meters, and ε_o is the permittivity of a vacuum (8.85×10^{-12} farads/meter).

1.2 Cube

The capacitance of an isolated cube has been found to be[2,3]

$$C_{ISO} = 4\pi\varepsilon_o (0.656) \ell \tag{A2}$$

where ℓ is the length of the sides of the cube in meters and C_{ISO} is expressed in farads.

1.3 Cylinder

The capacitance of an isolated cylinder is given by[*]

$$C_{ISO} = \frac{4\pi\varepsilon_o a}{\ln\left[\dfrac{a + (a^2 + R^2)^{1/2}}{R}\right]} \tag{A3}$$

where C_{ISO} is expressed in farads, a is one-half the length of the cylinder in meters, and R is the radius of the cylinder in meters.

---

[*]This formula was derived by the authors.

1.4 Truncated Cone

The capacitance of a truncated cone will be approximated by the capacitance of a cylinder with a length equal to that of the cone, but the radius of the equivalent cylinder is the average of the radii of the truncated cone. Using Eq. (A3), the results are

$$C_{ISO} \cong \frac{4 \pi \epsilon_o a}{\ln \left[\dfrac{a + (a^2 + \hat{R}^2)^{1/2}}{\hat{R}} \right]} \tag{A4}$$

where $\hat{R} = (R_1 + R_2)/2$ and C_{ISO} is expressed in farads and the radii expressed in meters.

1.5 Thin Rectangular and Elliptical Plates

The capacitance of thin rectangular and elliptical plates have been derived in a previous paper[5] and the results are given in graphical form for various values of length and width, and semimajor and semiminor axes, respectively.

1.6 Thin Circular Plate

The capacitance of a thin circular plate is given by[4]

$$C_{ISO} = \frac{2R}{\pi} (111.1) \tag{A5}$$

where R is the radius of the circular disk in meters and C_{ISO} is in picofarads.

References

1. Kraus, J. D. (1953) Electromagnetics, McGraw-Hill Co., New York.
2. Van Bladel, J. (1964) Electromagnetics Fields, McGraw-Hill Co., New York.
3. Reitan, D. K., and Higgins, T. J. (1951) Calculation of the electrical capacitance of a cube, J. Appl. Phys. 22:223-226.
4. Reitan, D. K., and Higgins, T. J. (1956) Accurate determination of the capacitance of a thin rectangular plate, Trans. Am. Inst. of Electrical Engineers 75:pt. 1.